FILE COPY

OFFICE MEMORANDUM

LOS ALAMOS SCIENTIFIC LABORATORY
UNIVERSITY OF CALIFORNIA
LOS ALAMOS, NEW MEXICO 87545
Telephone Ext:

TO : Distribution

DATE: April 21, 1980

FROM : L. Aamodt and G. Zyvoloski

SUBJECT : REPORT ON PHASE 1, SEGMENT 5, STAGE 1 (START-UP OF EXPERIMENT 217)

SYMBOL : G-5/#5/80

MAIL STOP:

(See attached)

FILE COPY

REPORT ON PHASE 1, SEGMENT 5, STAGE 1
(START-UP OF EXPERIMENT 217)

Lee Aamodt and George Zyvoloski

INTRODUCTION

Experiment 217 is a long-term (3 to 6 months) heat extraction experiment in the new EE-1/GT-2B circulation system, with flow entrance at 2.93 km (9620 ft) depth and flow exit in the open hole section of GT-2B which extends from 2.61 km (8550 ft) to 2.71 km (8900 ft) depth. In order to characterize the fracture system as the experiment began, some parameters which have been shown to be flow and pressure dependent were measured at various flow rates and pressure levels, with flow injection into GT-2B as well as EE-1.

A list of these constant-flow experiments is given in Table I

Table I
Stage one constant flow

	Flow rate	Injection Well
1	0.57 ℓ/s (9 GPM)	GT-2B
2	2.14 ℓ/s (34 GPM)	GT-2B
3	0.57 ℓ/s (9 GPM)	EE-1
4	2.14 ℓ/s (34 GPM)	EE-1
5	3.47 ℓ/s (55 GPM)	EE-1
6	5.05 ℓ/s (80 GPM)	EE-1
7	6.94 ℓ/s (110 GPM)	EE-1

Two parameters of especial interest are the quantity $A\sqrt{k}$ (area x square root of permeability) and the impedance, defined as the output flow divided by the pressure drop across the fracture. At low flow rates inertial effects along the flow path are negligible, but as the velocity increases they become more important and impedance increases with flow rate. However, when the pressure becomes sufficiently high to increase the fracture width, this effect may cause a reduction in impedance that overrides the increase due to flow rate.

RESULTS

The first four flow tests in Table I were conducted with KOBE constant displacement pumps, and the flow rate was well defined. When pumping into GT-2B, the starting pressure was well defined at a few psi (it had been shut in for six days after prolonged venting). Because of a difference in the average temperature in the two wellbores, the colder EE-1 water column was ∿ 12.2 m (40 ft) below the surface, corresponding to a negative pressure of 1.2 bar (17 psi) at the surface. When pumping into EE-1 began, an attempt was made to condition the EE-1 well to zero surface pressure by filling it before pumping began. Since this caused a transient in the flow data, the small flows into EE-1, where a few psi were important, were difficult to analyze (no measurement of $A\sqrt{k}$ was made on the smallest EE-1 flow).

Plots of pressure vs. time and flow rate vs time for all seven constant flow tests are given in Fig. 1 to Fig. 8.

ANALYSIS

Initial pressure rise. When a large planar fracture, across which the impedance is negligible, is pressurized by a constant rate input flow,

permeation may be taken as normal to the face, i.e., one-dimensional, and the pressure is expected to rise linearly with the square root of pumping time.[1] Such behavior has often been observed and has been used to evaluate the parameter $A\sqrt{k}$, where A is twice the fracture area and k is the permeability of the rock. We will designate this model as model A. An alternative view of these experiments has recently been proposed by H. Fisher, i.e., that the area A is not the area of the fracture faces but the distance separating the faces times the fracture width, while k is the permeability along the fracture, rather than that into the fracture face. In this view the one-dimensional nature of the diffusion is due to parallel joints which fix the fracture width, so that the flow path quickly becomes one-dimensional -- both the fracture-face separation and permeability along the face must, on the average, be constant in this model, which we call model B. Since, in the real world, diffusion of both types must occur (although diffusion along the fracture could equally well be radial), the difference between the two models must be largely one of time constants, and if both time constants were similar, a combination of both effects might be expected.

Observable differences in the two models. In model A, the value of $A\sqrt{k}$ at low pressure should be the same, at a given flow rate, whether the fracture is inflated from GT-2B or EE-1. The value of $A\sqrt{k}$ should also vary little with flow rate, since flow rates into the rock over a large area will be slow and no inertial effects are expected.

In model B, the area is much smaller, k is greater, and variations of k with flow rate are shown to occur by the variations of impedance with flow given in the next section. Similarly, there is no good reason to expect $A\sqrt{k}$ to look the same from the GT-2 and EE-1 entrance points, since their geometries are probably quite different.

Model used for $A\sqrt{k}$ analysis and results. The computer program PUMPR used to analyze the initial pressure rise employs a one-dimensional diffusion code with a wellbore storage term $\frac{dV}{dP}$ (i.e., βV) followed by an entrance impedance R and the linear diffusion, where V is wellbore volume, P is wellbore pressure, and β is the compressibility of water. Although the data were fitted rather well by this model, the interpretation of these parameters in practice is not as simple as given above, e.g., the wellbore volume for $\beta V = 0.04\ m^3/bar$ is 800 m^3 (211,000 gal), about ten times the actual wellbore volume. It appears that some fracture compressibility must be included in this volume -- if a fracture compressibility of 0.03 MPa^{-1} is assumed[2], a volume of 13 m^3 (3400 gal) in the fracture is required. In spite of this compressibility problem, the flow dependence of R and the $A\sqrt{k}$ values derived from this code show reasonable consistency. Figures 9 through 13 show the agreement between calculations and experimental data for all but the third and sixth flow tests, where data was too poor to attempt a fit.

Table II gives the results of these calculations.

It is seen that except for the lowest flow rate into GT-2B, the results are most consistent with model A, i.e., the $A\sqrt{k}$ values appear to be independent of flow rate and flow direction. In the two GT-2B runs, the value

Table II

Measured Parameters in Transient Start-up Tests

Flow ℓ/s	gpm	Entrance Well	βV	R bar s/ℓ	psi/gpm	$A\sqrt{k}(cm^3)$
0.57	9	GT-2B	0.04	2.92	2.67	1430
2.15	34	GT-2B	0.035	4.85	4.44	850
2.15	34	EE-1	0.04	0.96	0.875	970
3.47	55	EE-1	0.035	4.39	4.0	850
6.62	105	EE-1	0.02	6.6	6.0	650

of $A\sqrt{k}$ varies inversely as the value of R, rather than the square root of R. It is possible that model B, or a combination of A and B, is effective at this low flow rate. Other models should be fitted to the data to see if they are less ambiguous.

IMPEDANCE

The determination of impedance is of primary importance to the economic feasibility of the HDR energy extraction scheme. Flowing water at various rates and directions gives information on the flow dependence and location of the system impedance. The impedance calculated from wellhead measured quantities contains buoyancy effects which must be accounted for if accurate flow dependance relationships are to be established. To calculate the buoyancy contribution to the pressure difference, the code WBHT was used. This code simulates the transfer of heat to or from the fluid flowing in the wellbore. A description of the code is given in a memo by G. Zyvoloski (Aug. 28, 1979). The input values to the code are given in Table III. The buoyancy corrections as a function of time are given in Figures 14-17. To the low flow rate curves (Figs.14 and 15) must be added the initial buoyancy as given by the depth differences before flowing between the two wellbores. This amounted to approximately 1.2 bar (16 psi). The buoyancy corrected values of the impedance are given in Figs. 18-21. A summary of the quasi steady-state impedances, wellhead pressures, and flow rates are presented in Table IV.

Table 3

Input parameters for WBHT

Initial temperature distribution	- 35 + .0539L, where L is length down casing
Thermal conductivities:	
λ_{water}	- .66 W/M°K
λ_{rock}	- 2.9 W/M°K
λ_{steel}	- 36 W/M°K
Specific heats	
C_{water}	- 4.2×10^6 J/kg°K
C_{rock}	- $1. \times 10^6$ J/kg°K
Kinematic viscosity, γ	= $3. \times 10^{-7}$ m^2/sec
Density of rock	= 2700 kg/m^3
Pipe diameter	- .24 m (9-5/8 in.)
Reservoir extent	- 20 m (65.6 ft)
Reservoir depth	- 2926 m (9600 ft)
Finite difference cells radial direction	= 10
Finite difference cells, vertical direction	= 15
Time step increment	= 15 minutes

Table 4

Summary of Run Segment 5 Impedances

Pumping Well	(Pressure) hrs	psi	(GPM) q_{in}	(GPM) q_{out}	Corrected impedance (psi/gpm)
GT-2B	3.4	50	9	4.4	7.1
GT-2B	17.6	255	34	19.9	13.8
EE-1	0.28	4	9	7.1	2.8
EE-1	7.8	113	34	14.5	12.9
EE-1	43.1	625	55	19.1	30.5
EE-1	64.4	935	90	32.4	29.2
EE-1	91.7	1330	110	54	26.7

CONCLUSIONS

Although there are discrepancies which are still unexplained, a one-dimensional diffusion model with wellbore storage and an input impedance to the fracture can provide good fits to the transient pressure constant flow data generated in stage one of the Phase 1, Segment 5 flow test.

The data suggest that, at least at flow rates greater than 0.57 ℓ/s (9 gpm), the diffusion is into the face of the fracture, rather than along it.

As shown in Fig. 22, the flow dependence of impedance derived from the transient tests is very like that measured in the quasi-state impedance measurements. The impedance measured over much longer times is expected to decrease farther, as water losses from diffusion decrease and more flow reaches the fracture exit.

The flow dependence of impedance when flowing into GT-2B is less than tha observed when flowing into EE-1, perhaps because of the multiple entrance points in GT-2B vs one entrance point in EE-1. This would make velocities, and consequently, inertial effects, smaller in GT-2B.

Pressure dependence of impedance becomes important between 43 bars (625 psi) and 64 bars (935 psi) injection pressure (Table __ and Fig. 22). This appears low, but is not inconsistent with earlier data, i.e., Exp. 176 showed deviation due to pressure between 48 bars (700 psi) and 83 bars (1200 psi).

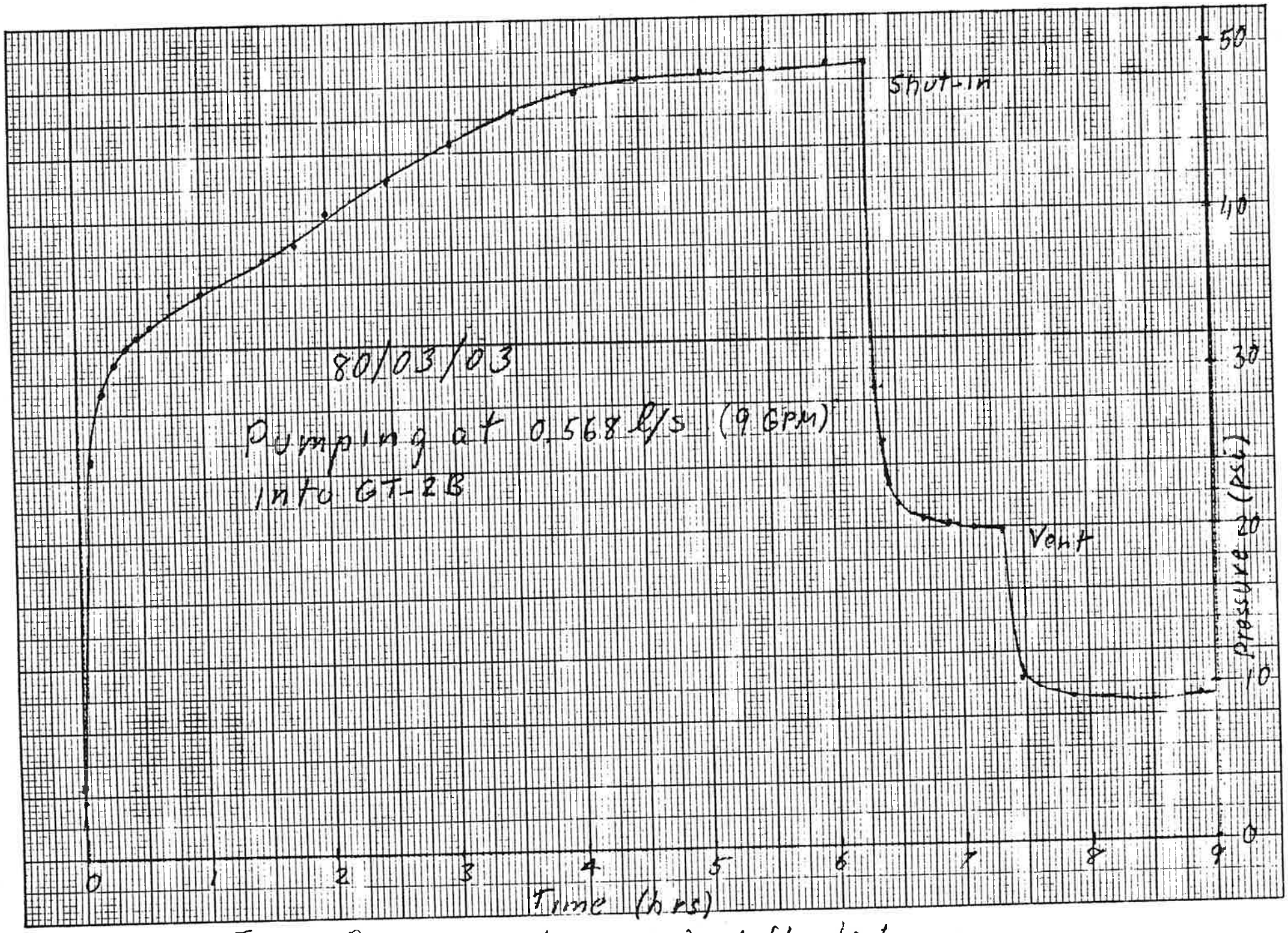

Fig. 1 Pressure vs time in first flow test.

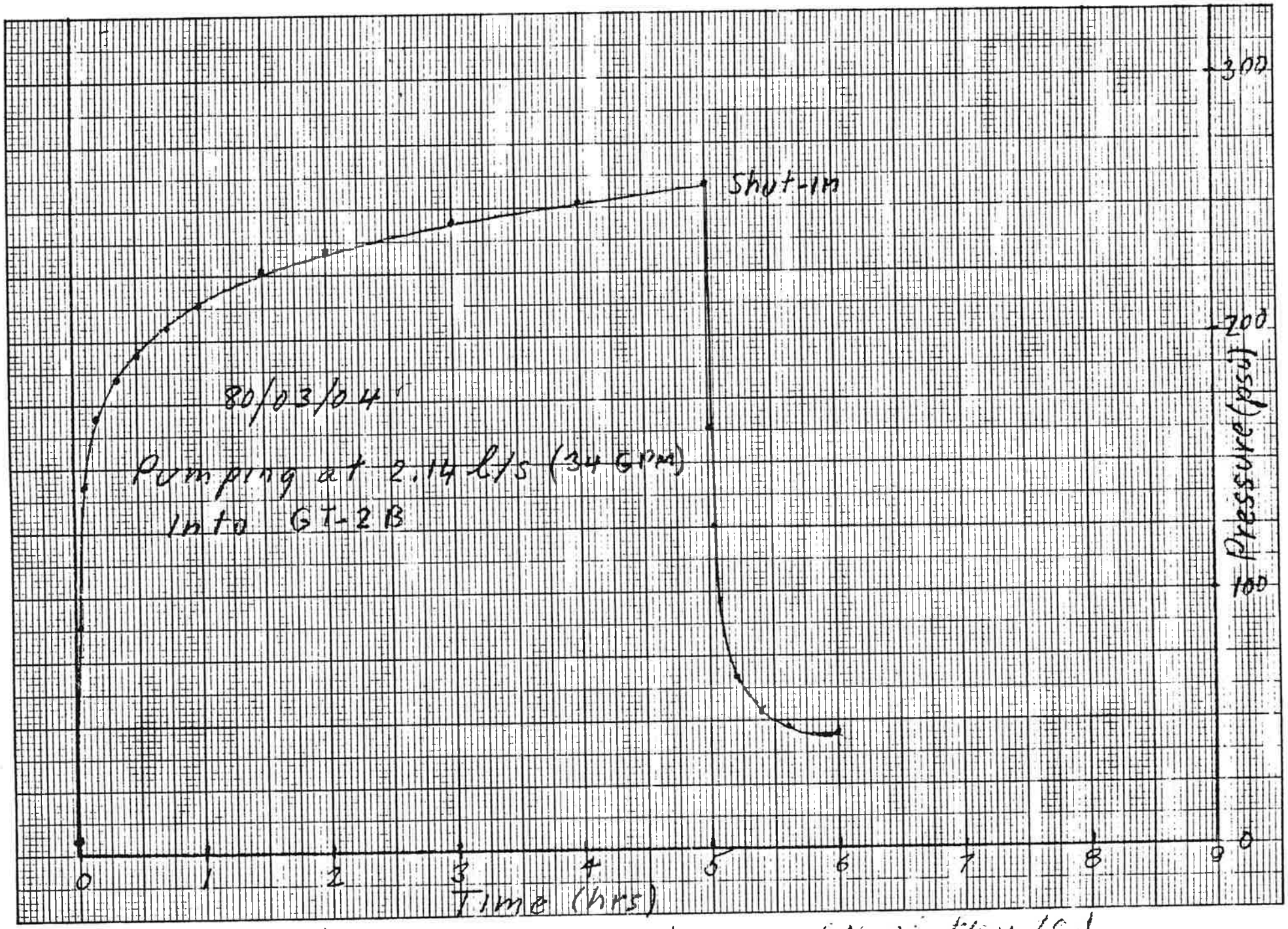

Fig. 2 Pressure vs time in second flow test.

K+E 10 X 10 TO 1/2 INCH 46 1323
7 X 10 INCHES MADE IN U.S.A.
KEUFFEL & ESSER CO.

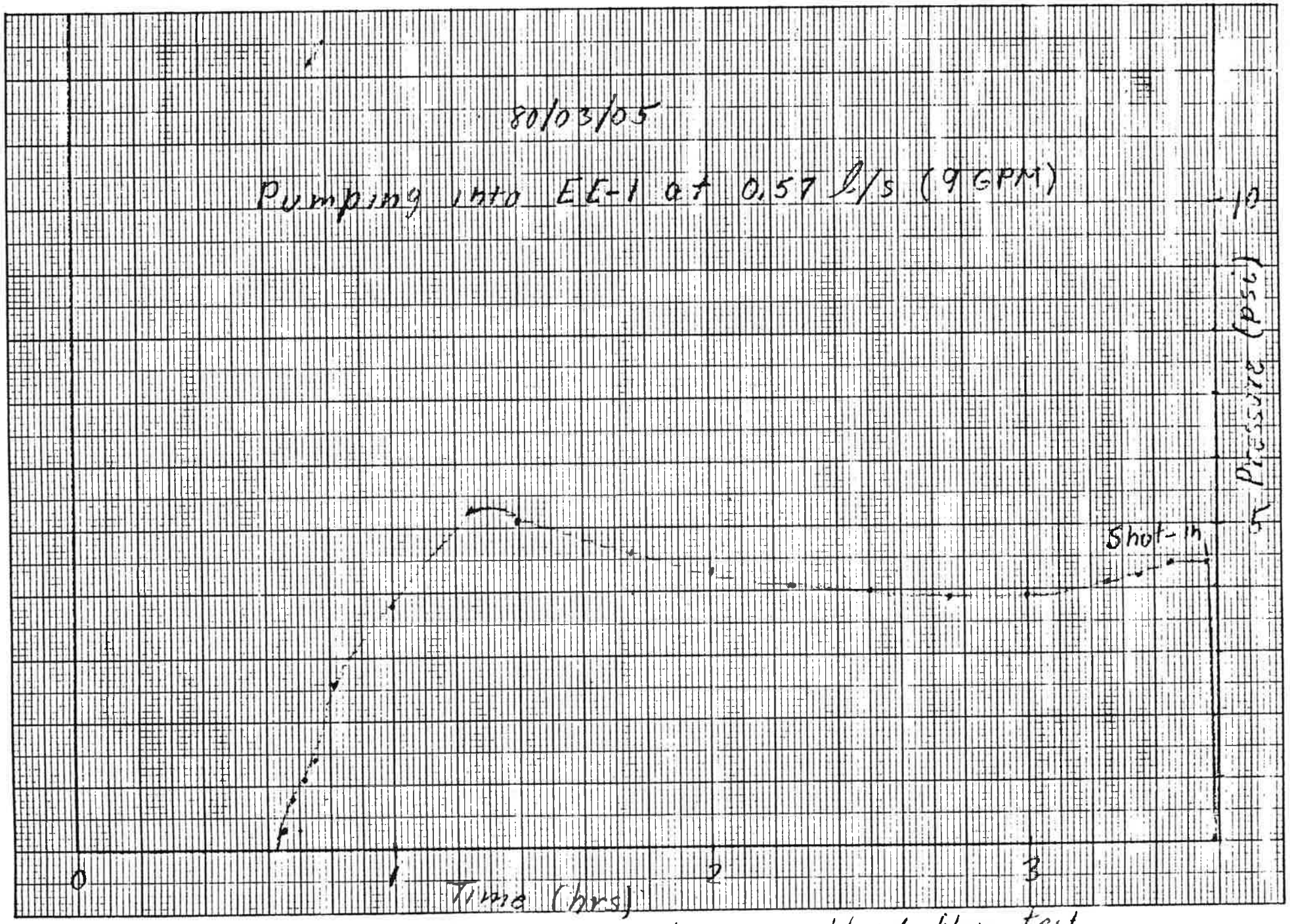

Fig. 3 Pressure vs time in third flow test.

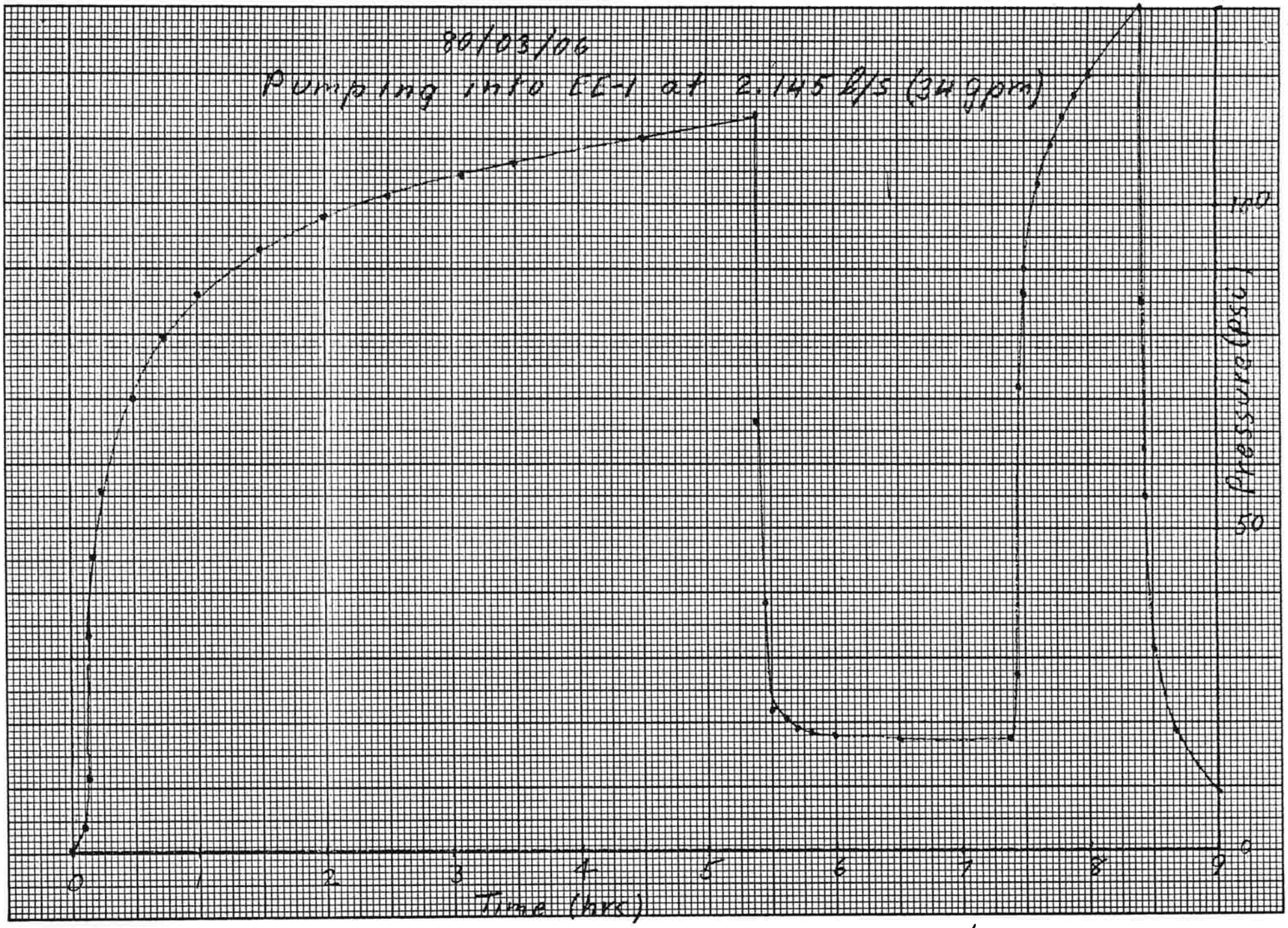

Fig. 4 Pressure vs time in fourth Flow test.

KEUFFEL & ESSER CO.
7 X 10 INCHES MADE IN U.S.A.

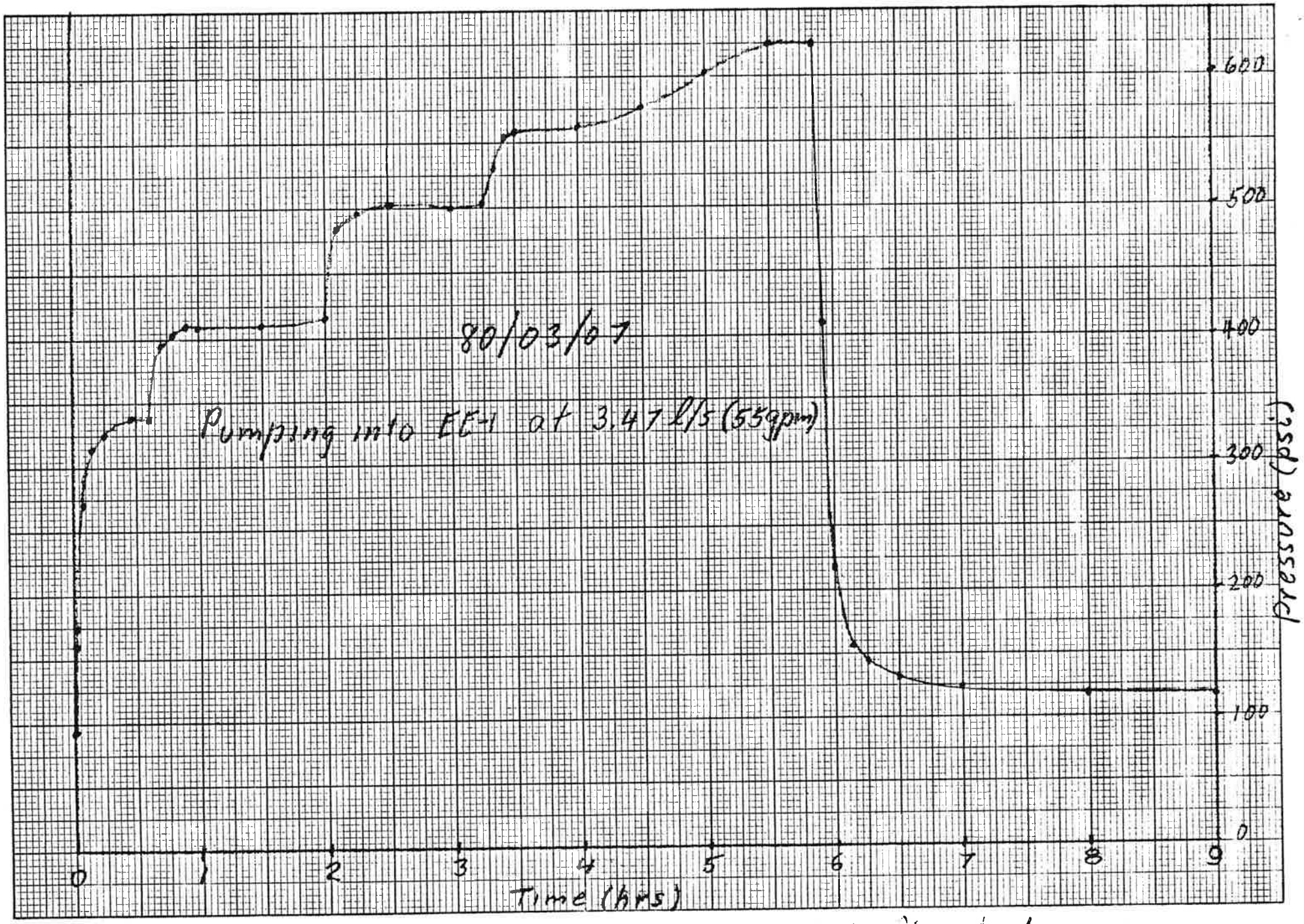

Fig. 5 Pressure vs time in fifth flow test.

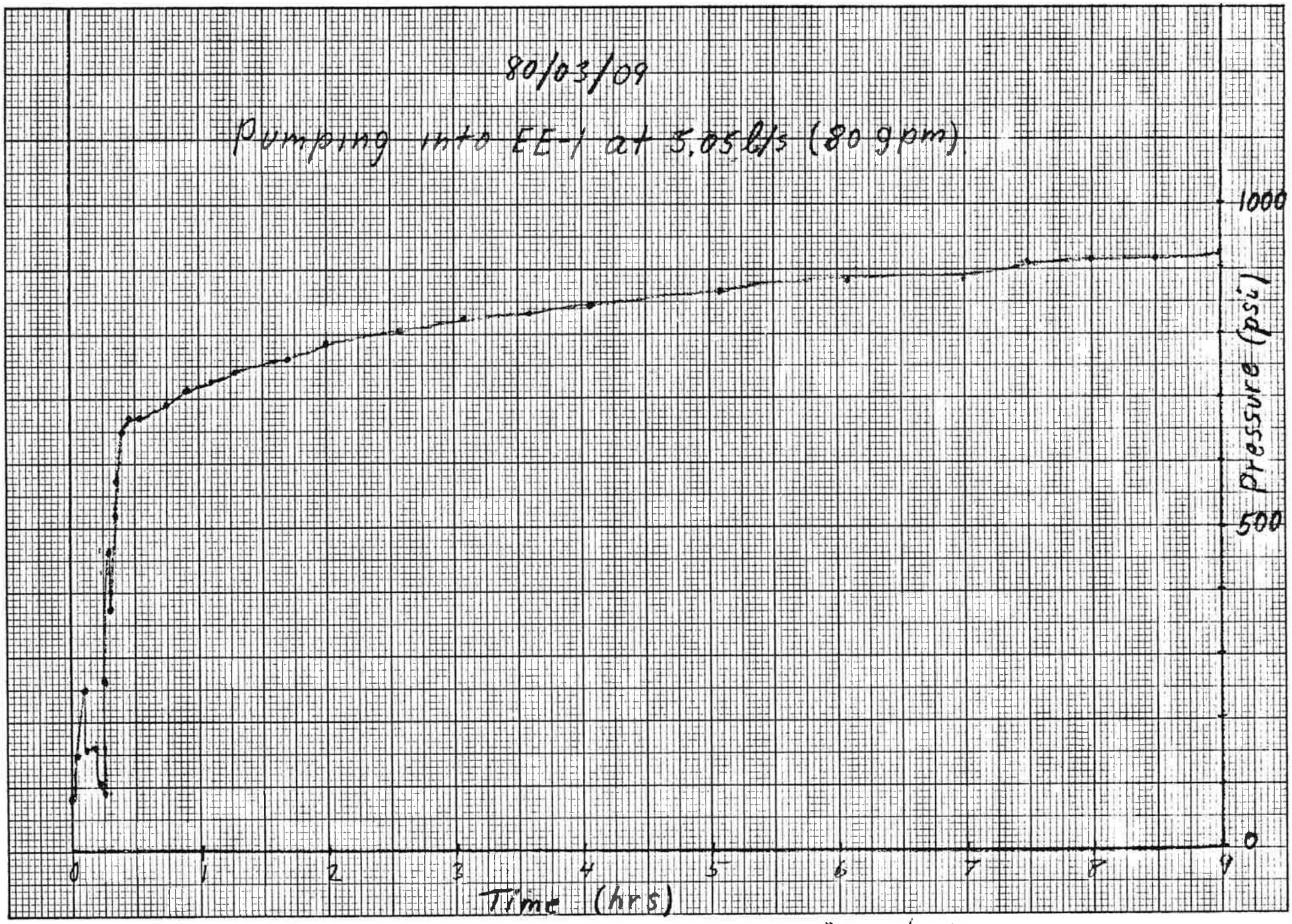

Fig. 6 Pressure vs time in sixth flow test.

K&E 10 X 10 TO ½ INCH 46 1323
7 X 10 INCHES MADE IN U.S.A.
KEUFFEL & ESSER CO.

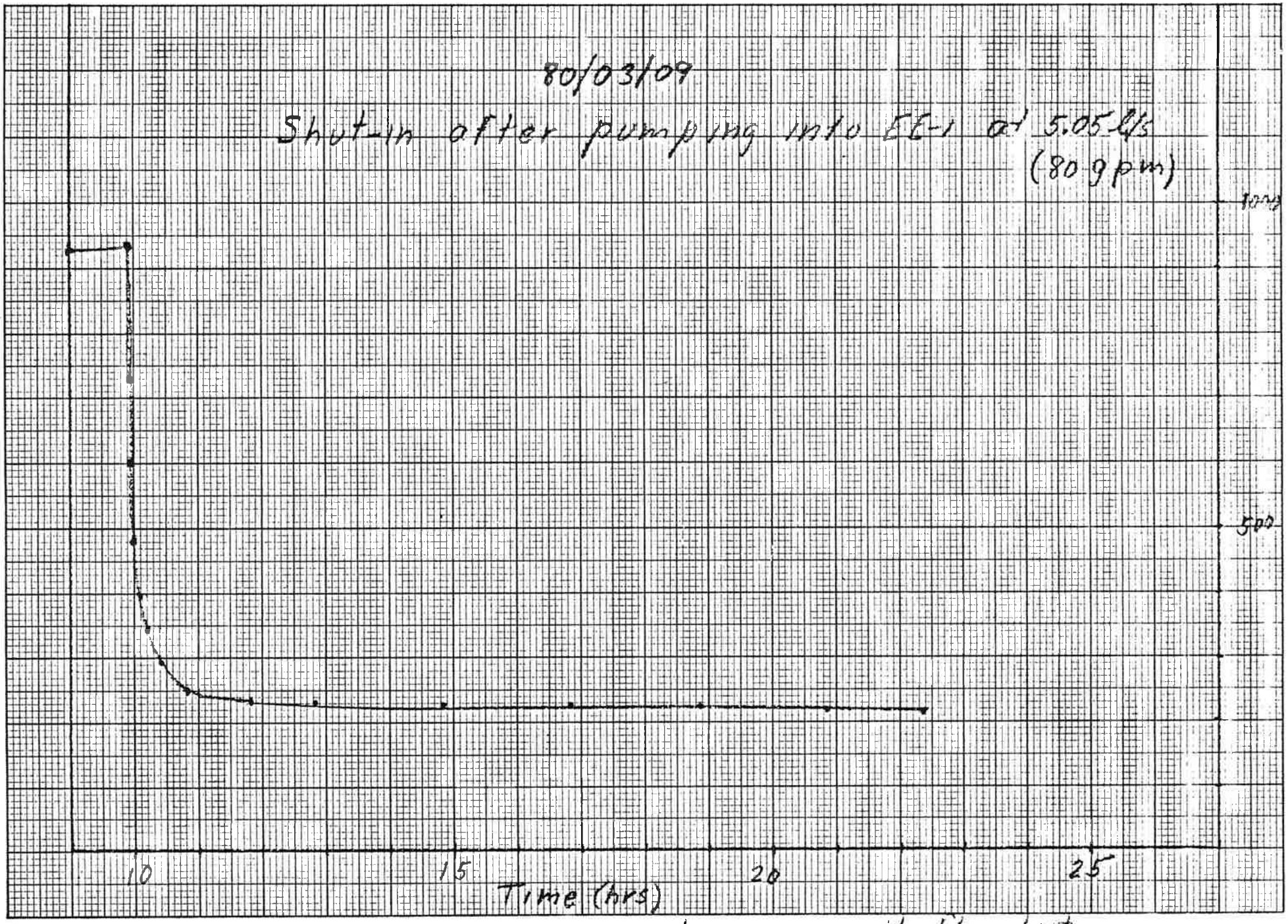

Fig. 7 Shut-in pressure vs time in sixth flow test.

K+E 10 X 10 TO ½ INCH 46 1323
7 X 10 INCHES MADE IN U.S.A.
KEUFFEL & ESSER CO.

Fig. 8 Pressure vs time in seventh flow test.

K+E 10 X 10 TO ½ INCH 46 1323
7 X 10 INCHES MADE IN U.S.A.
KEUFFEL & ESSER CO.

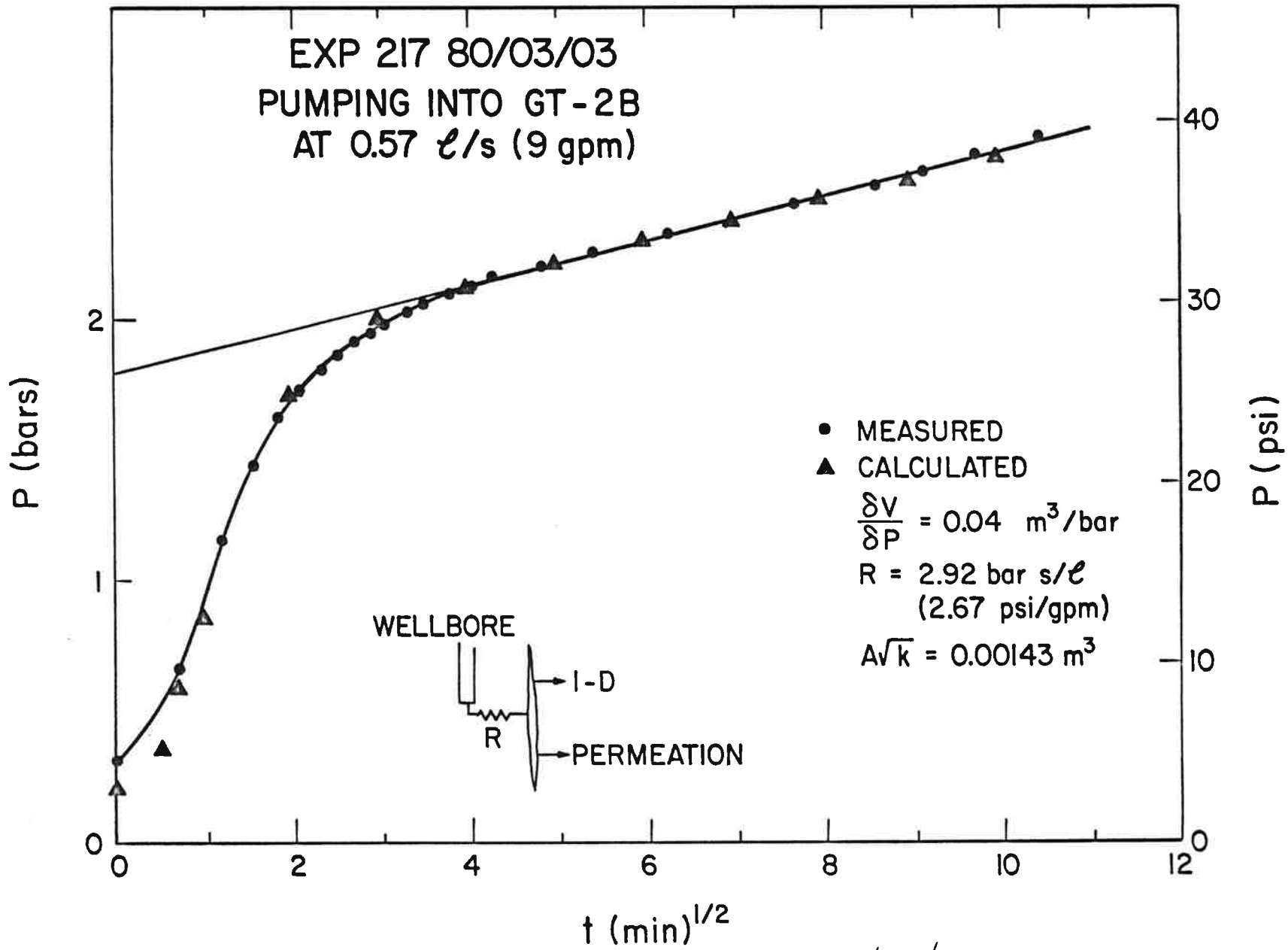

Fig. 9 Data fit in first flow test.

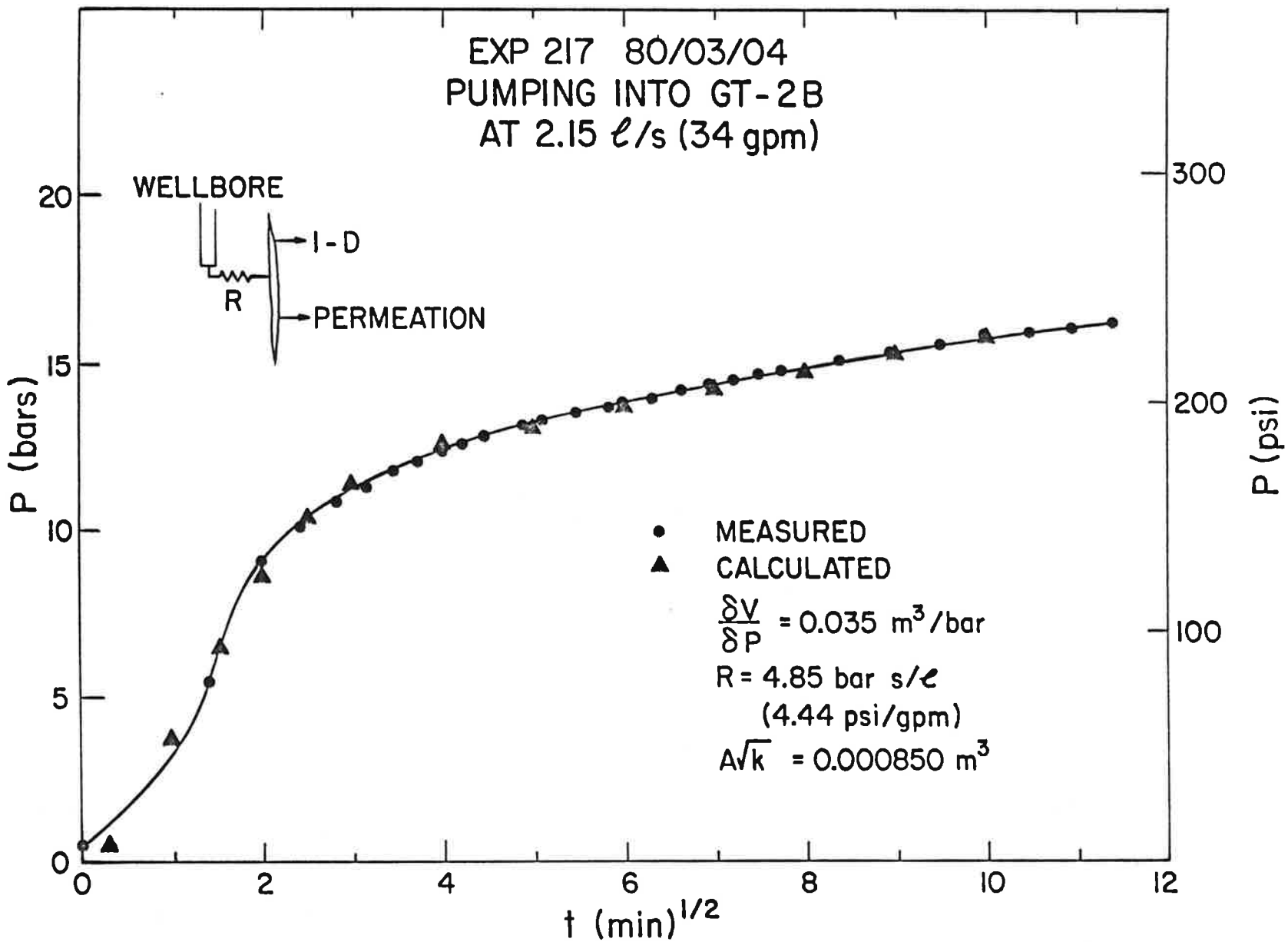

Fig. 10 Data fit in second flow test

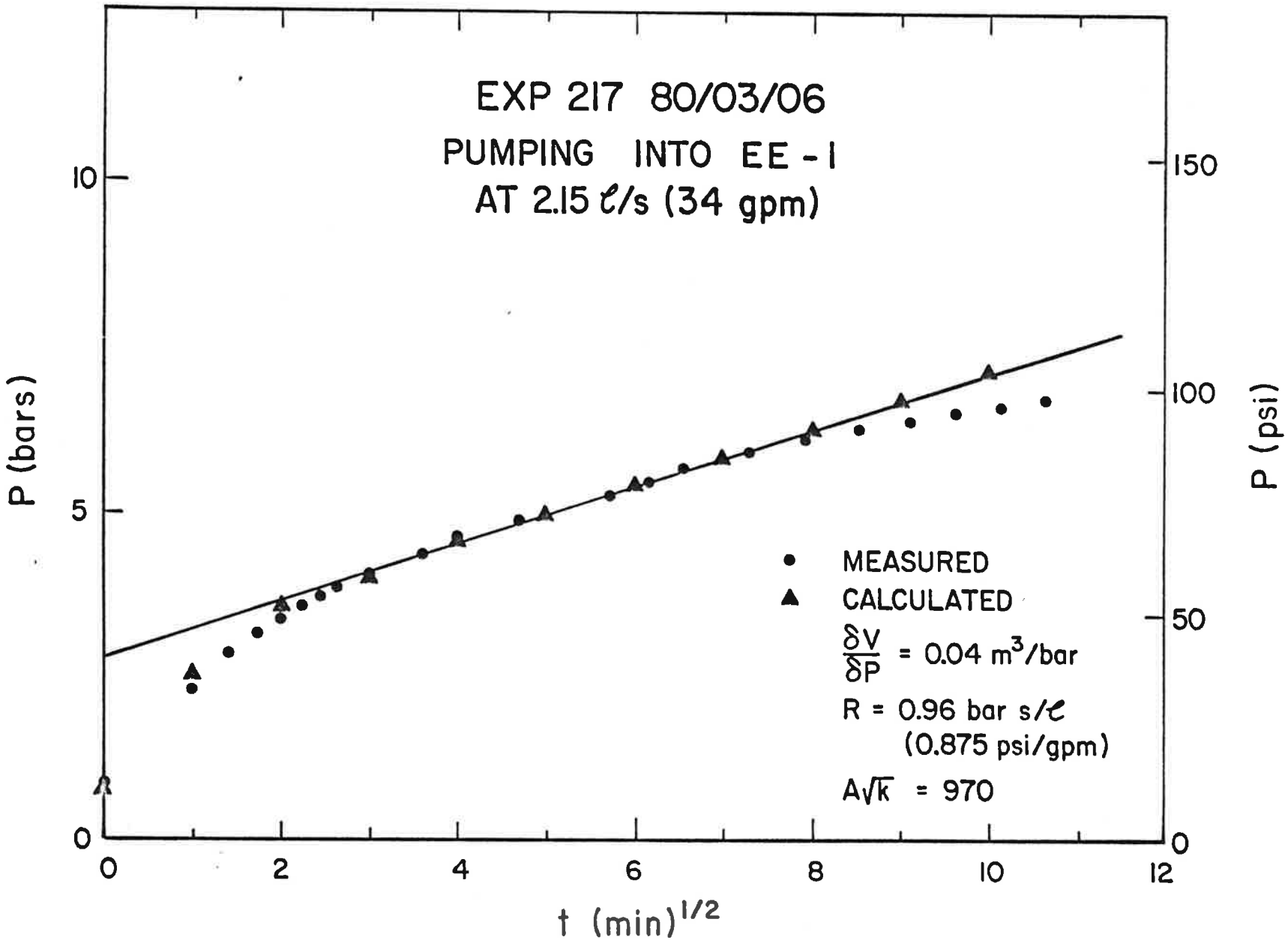

Fig. 11 Data fit in fourth flow test

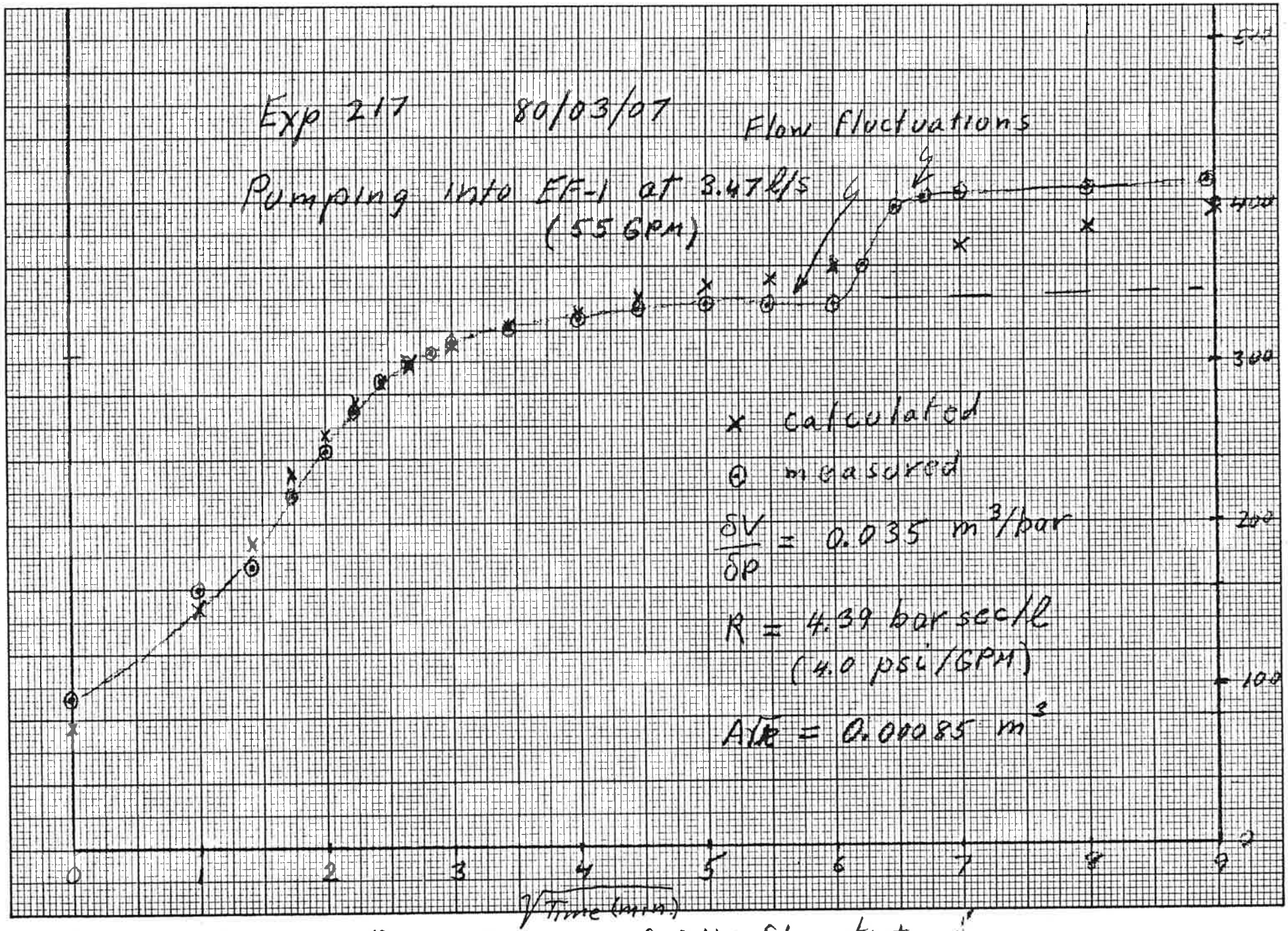

Fig. 12 Data fit in fifth flow test.

K+E 10 X 10 TO ½ INCH 46 1323
7 X 10 INCHES MADE IN U.S.A.
KEUFFEL & ESSER CO.

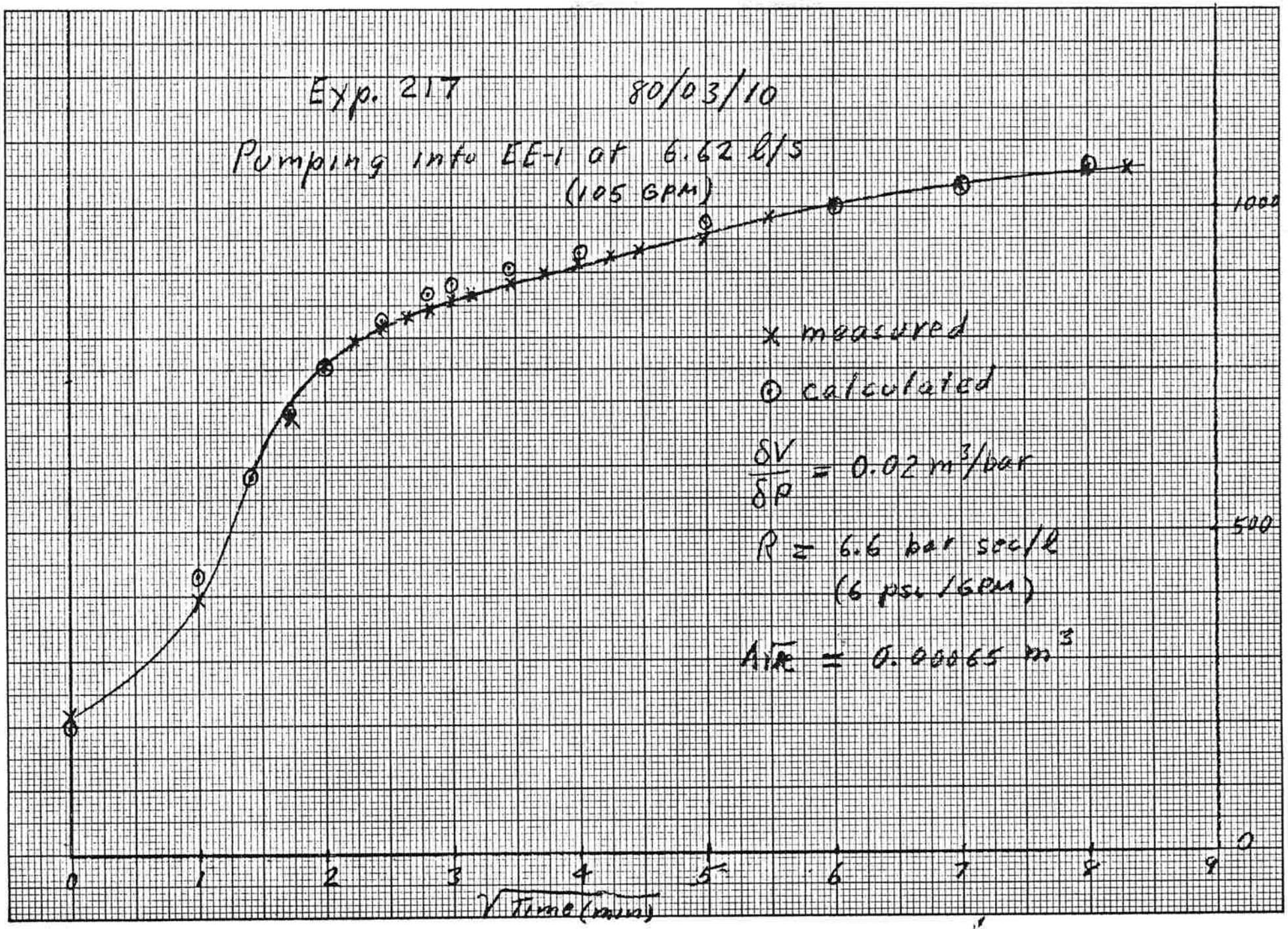

Fig. 13 Data fit in Seventh flow test.

K+E 10 X 10 TO ½ INCH 46 1323
7 X 10 INCHES MADE IN U.S.A.
KEUFFEL & ESSER CO.

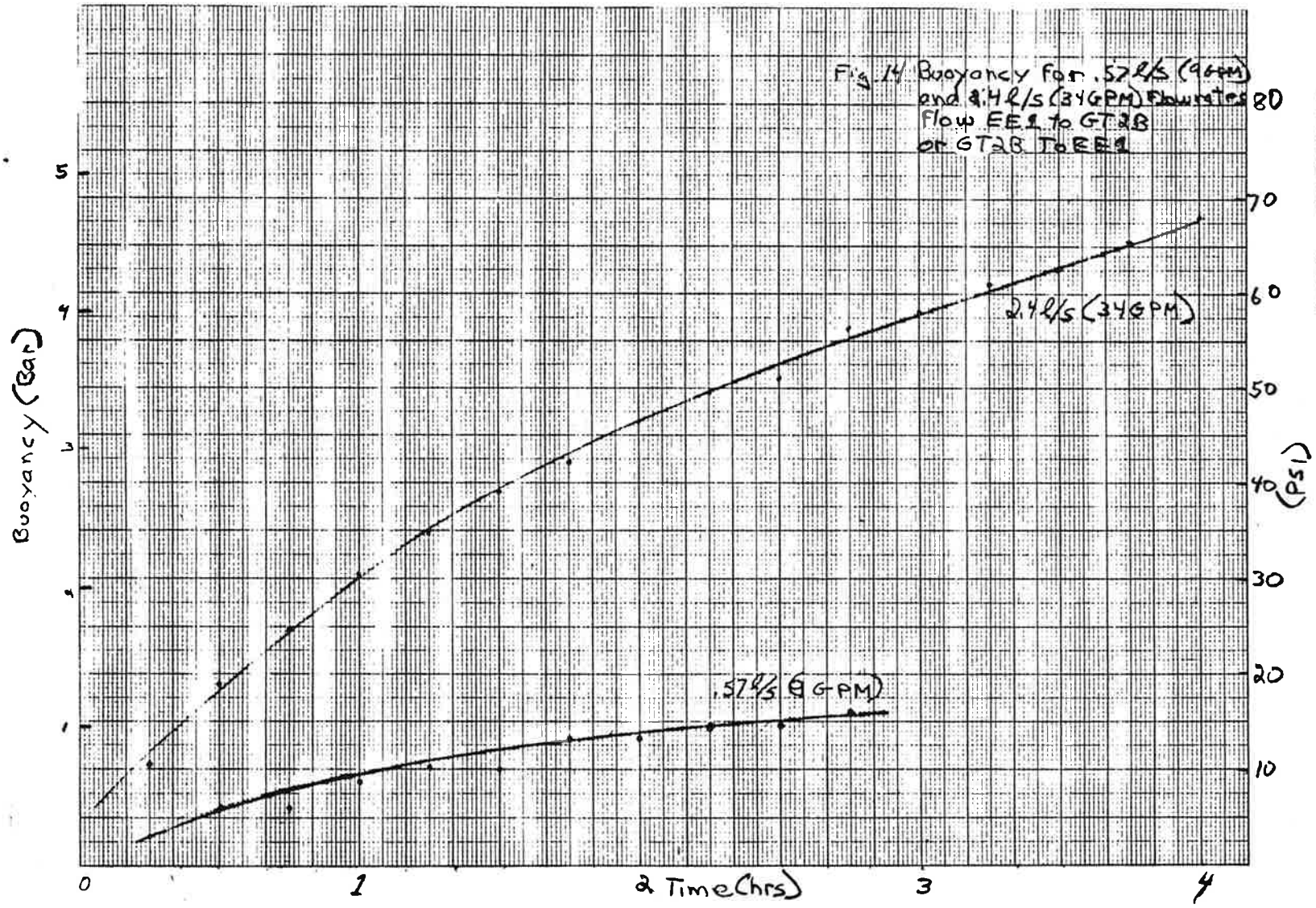
Fig. 14 Buoyancy For .57 l/s (9 GPM) and 2.4 l/s (34 GPM) Flowrates Flow EE1 to GT2B or GT2B To EE1
Buoyancy (Bar)
(PSI)
Time (hrs)
2.4 l/s (34 GPM)
.57 l/s (9 GPM)
0
1
2
3
4
5
10
20
30
40
50
60
70
80

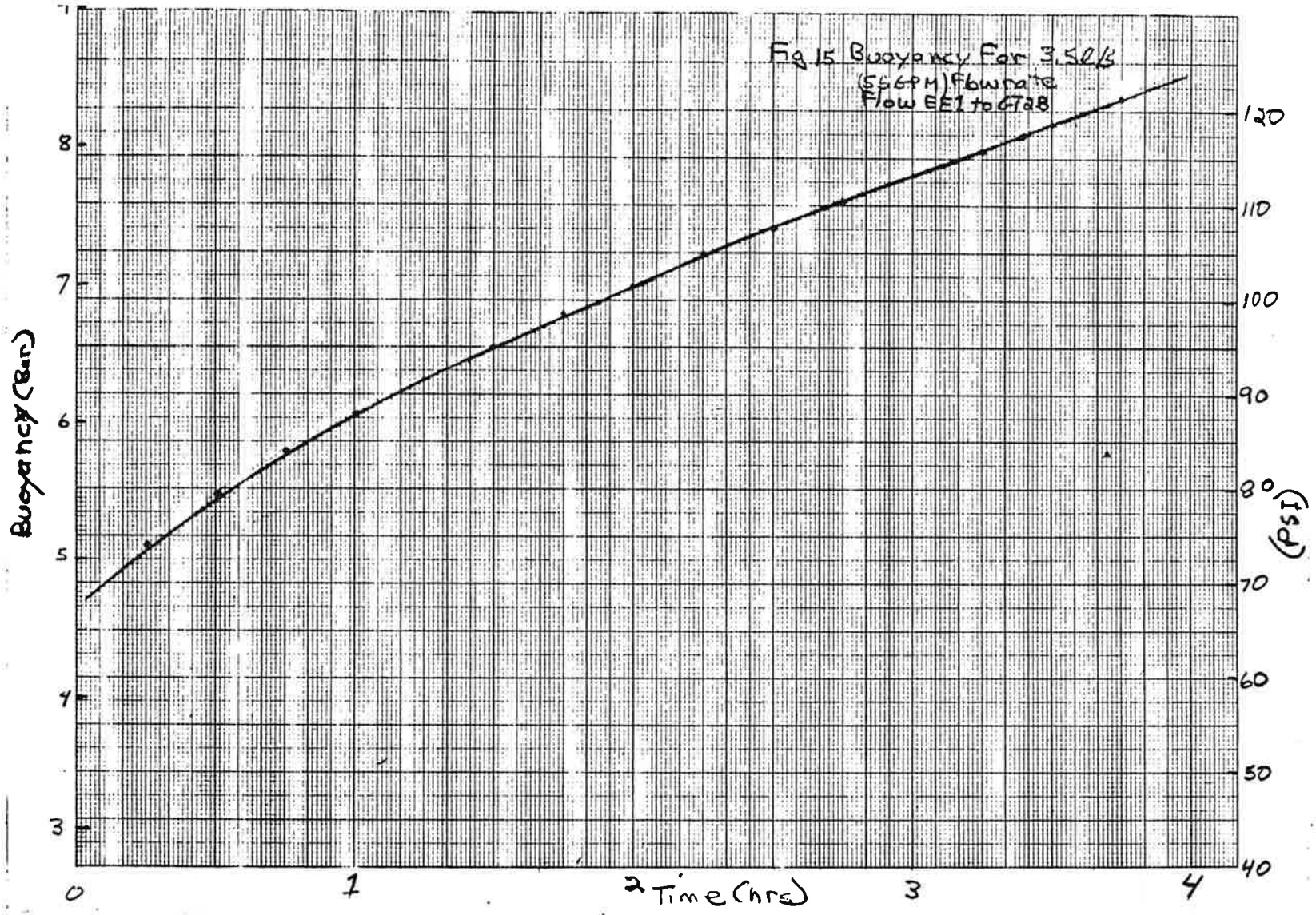
Fig 15 Buoyancy For 3.5 l/s
(55 GPM) Flowrate
Flow EE1 to GT2B
Buoyancy (Bar)
(PSI)
Time (hrs)
0
1
2
3
4
3
4
5
6
7
8
40
50
60
70
80
90
100
110
120

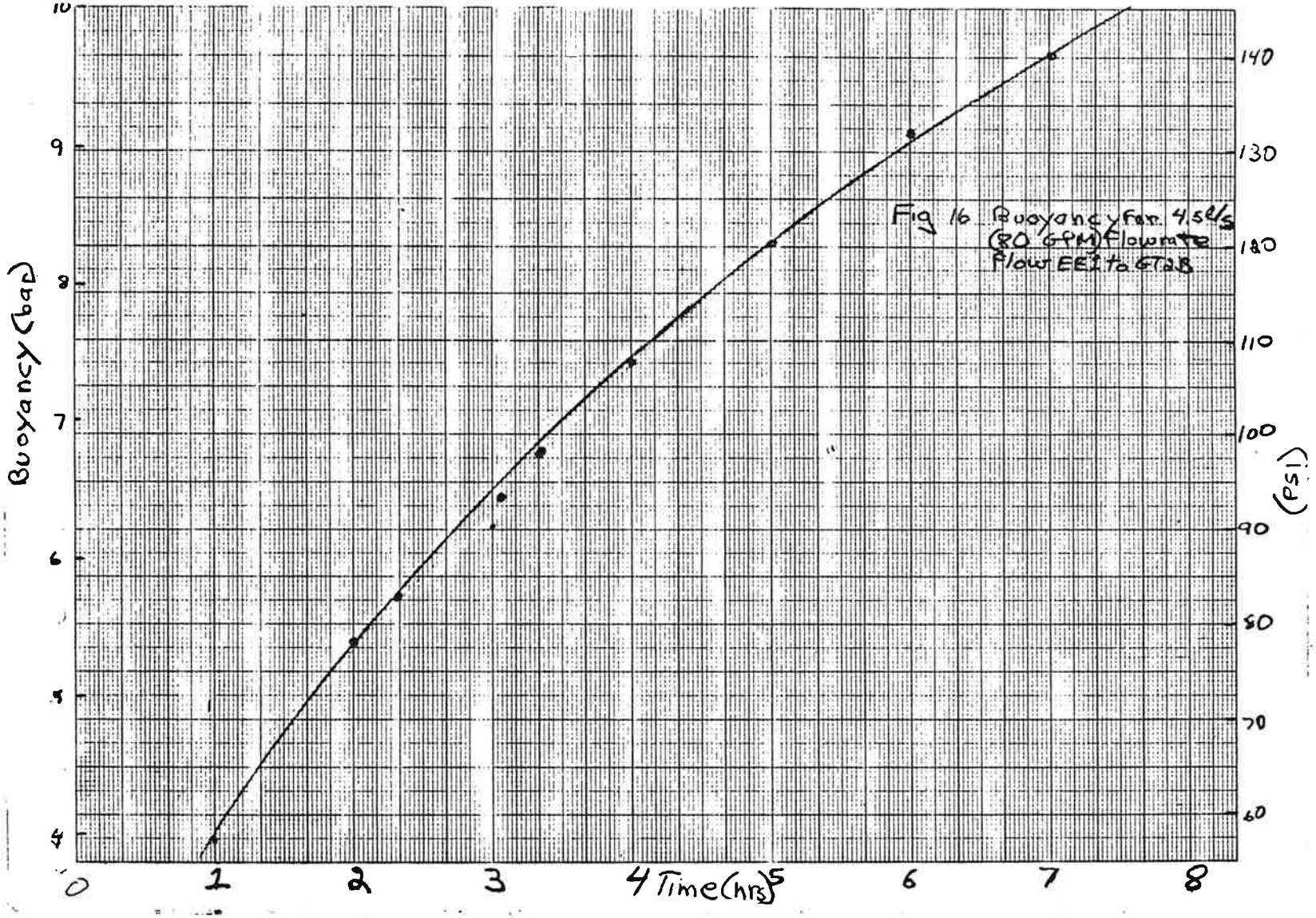

Fig 16 Buoyancy for 4.5 l/s (80 GPM) flowrate flow EE1 to GT2B

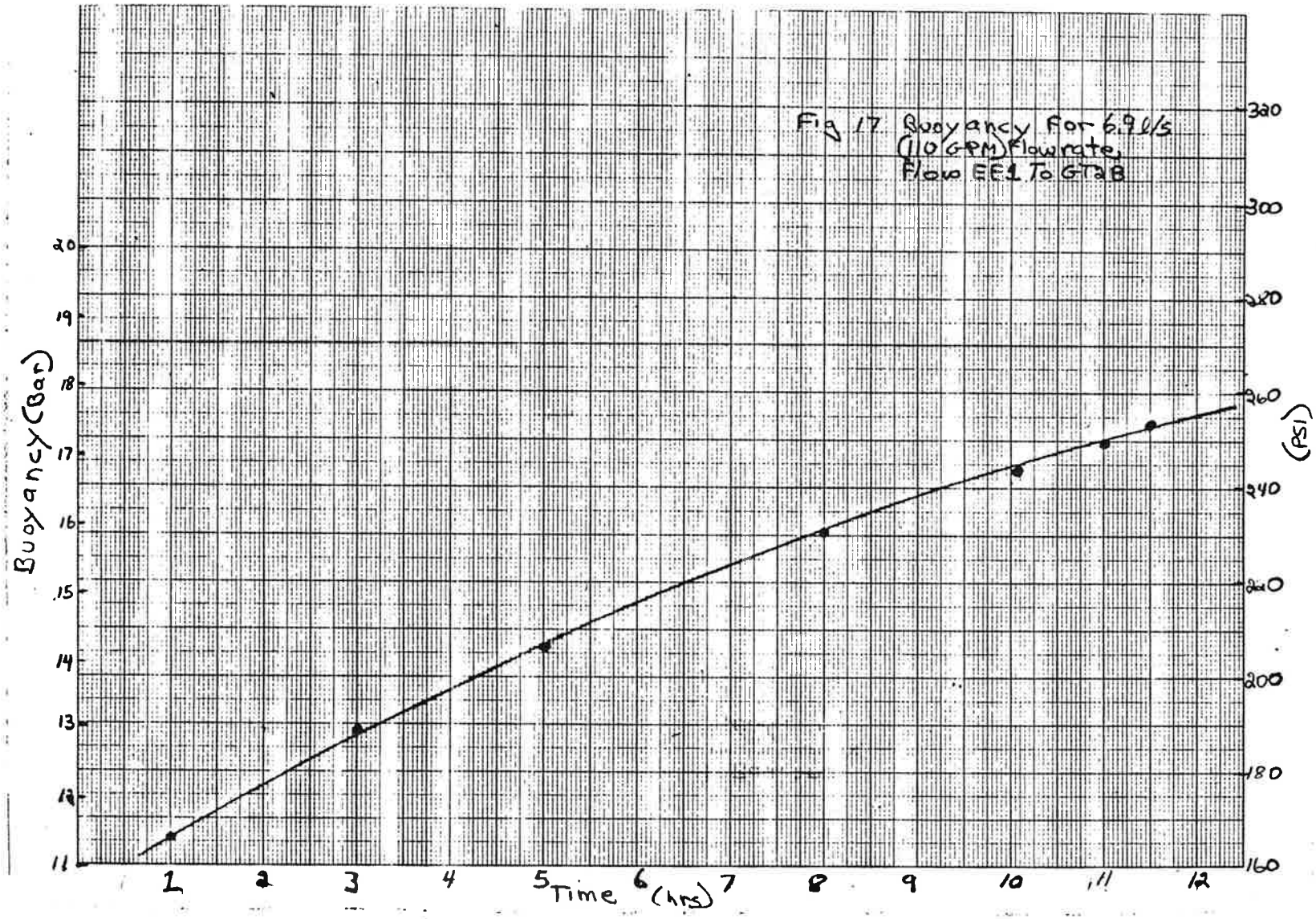

Fig 17 Buoyancy for 6.9 l/s (110 GPM) Flowrate, Flow EE1 To GT2B

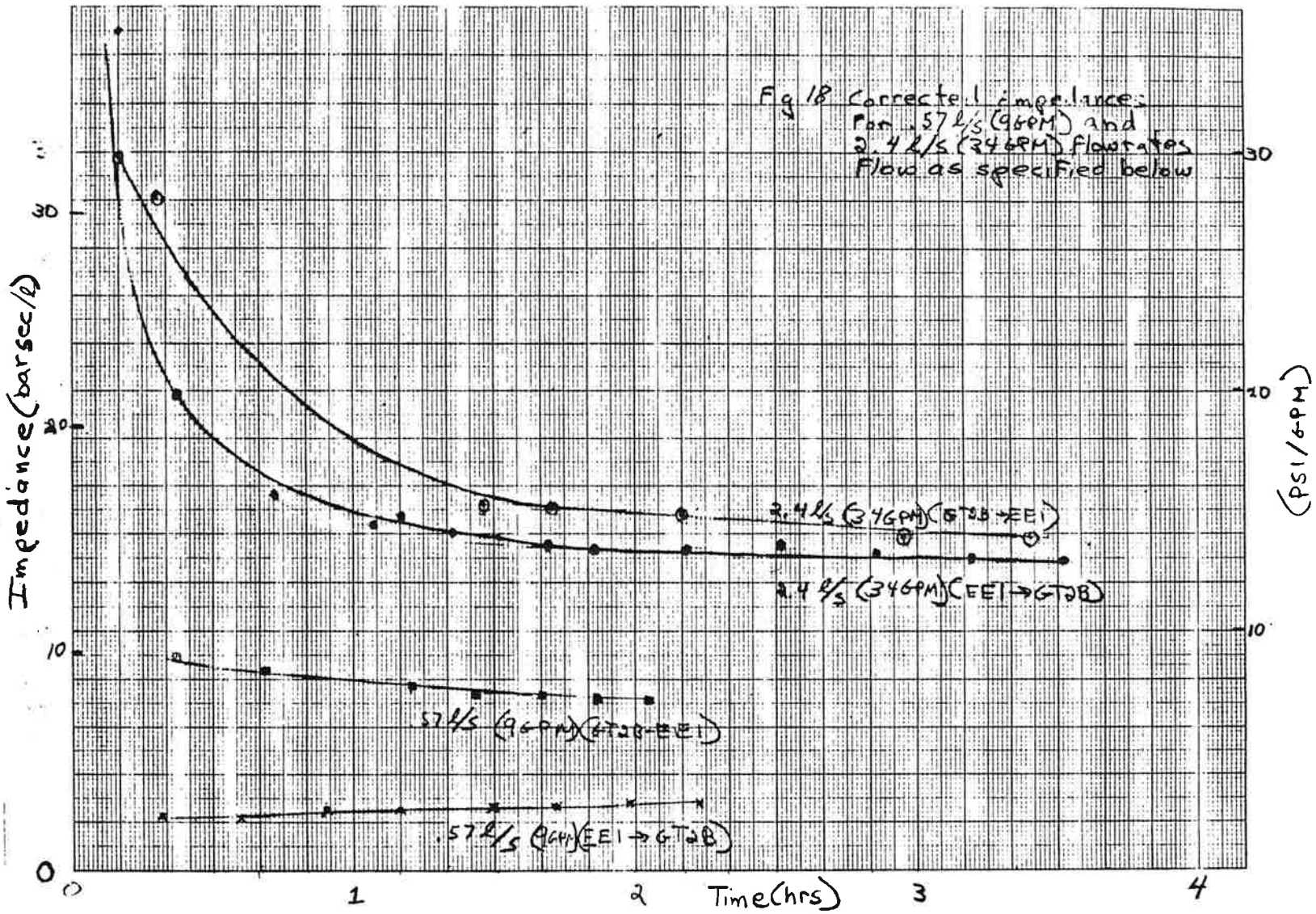
Fig 18 Corrected impedance:
For .57 l/s (9GPM) and
2.4 l/s (34GPM) flowrates
Flow as specified below
Impedance (barsec/l)
(PSI/GPM)
Time (hrs)
0
1
2
3
4
10
20
30
2.4 l/s (34GPM) (GT2B → EE1)
2.4 l/s (34GPM) (EE1 → GT2B)
.57 l/s (9GPM) (GT2B → EE1)
.57 l/s (9GPM) (EE1 → GT2B)

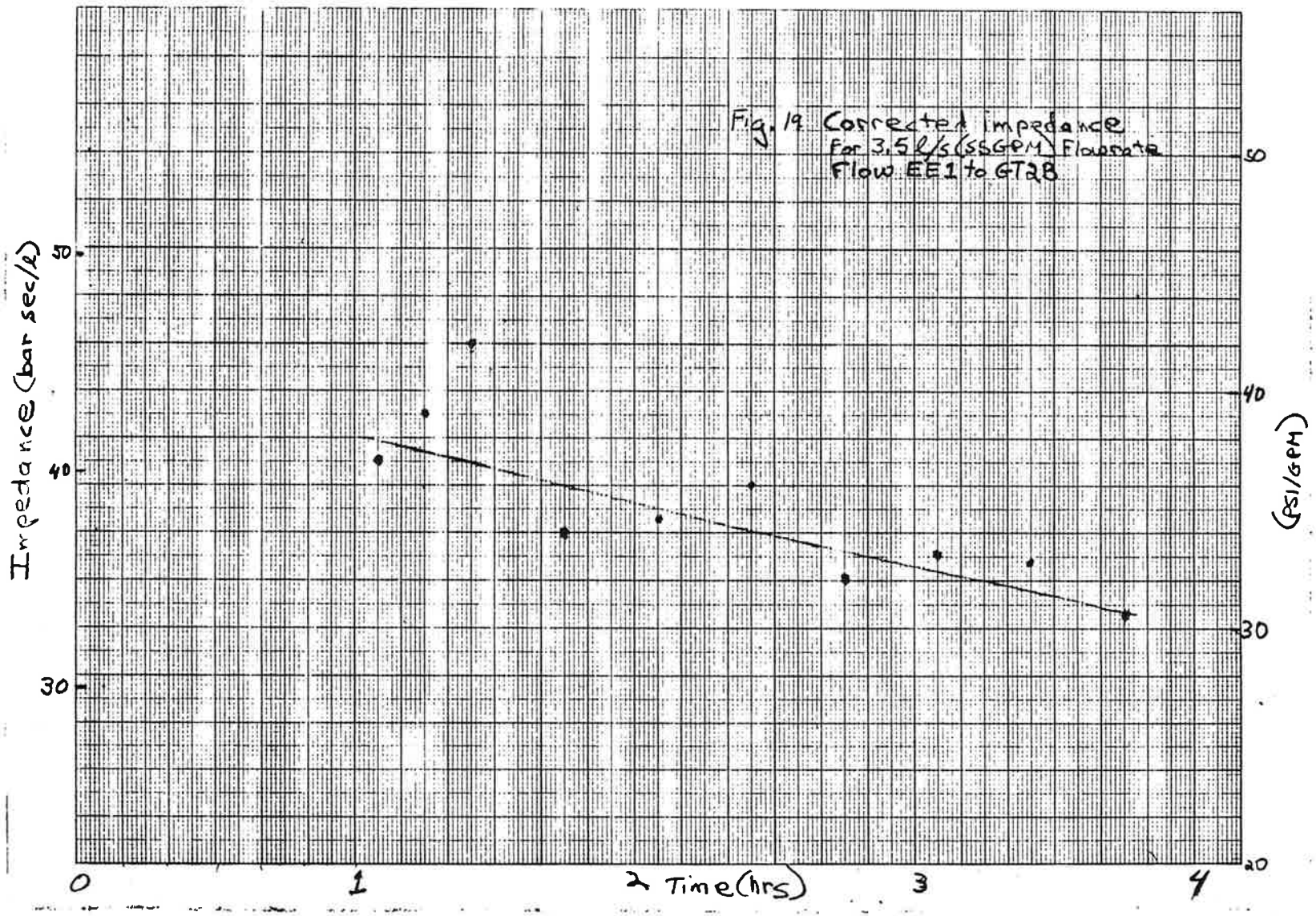

Fig. 19 Corrected impedance
For 3.5 l/s (55GPM) Flowrate
Flow EE1 to GT2B

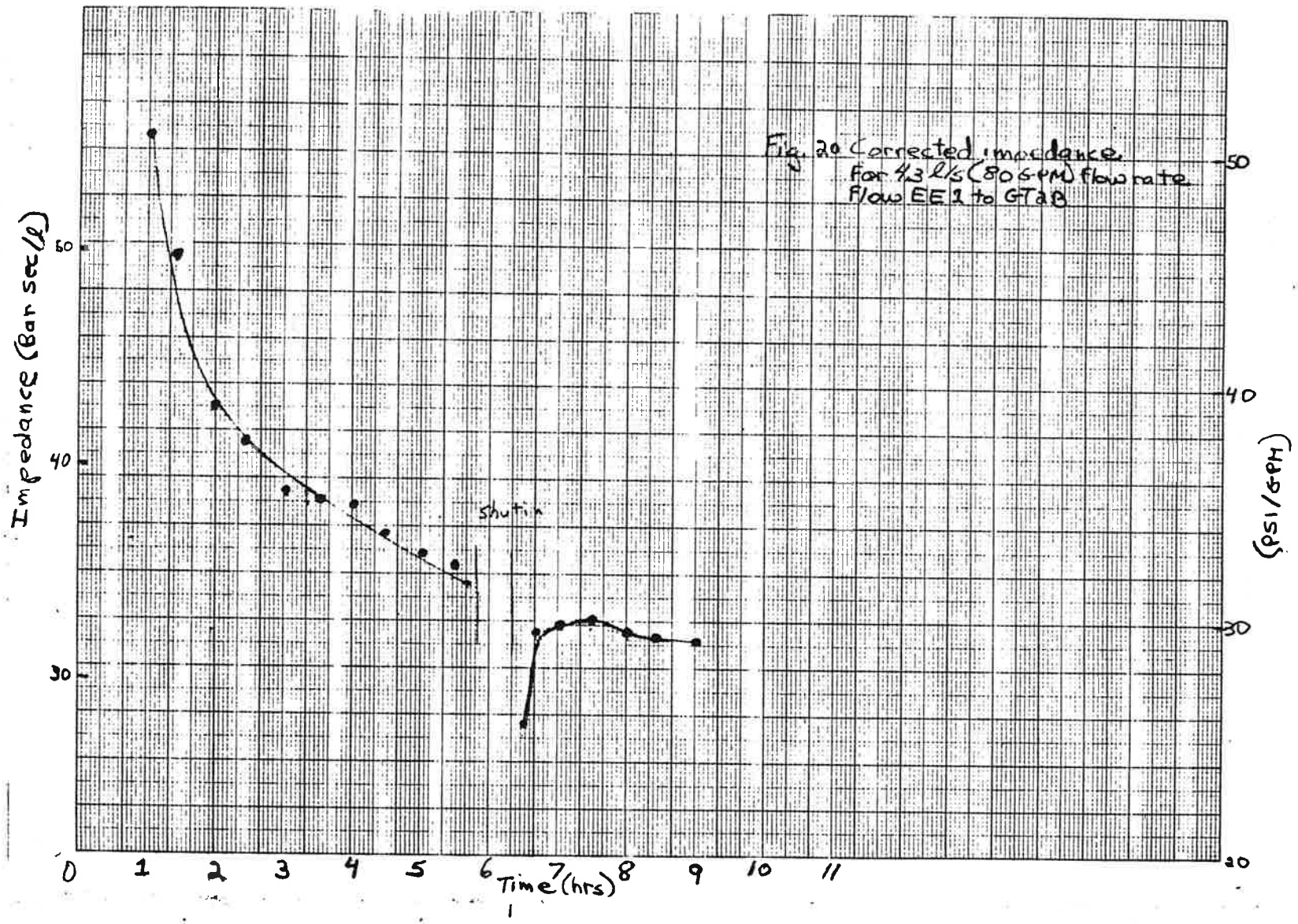

Fig. 20 Corrected impedance for 4.3 ℓ/s (80 GPM) flow rate Flow EE2 to GT2B

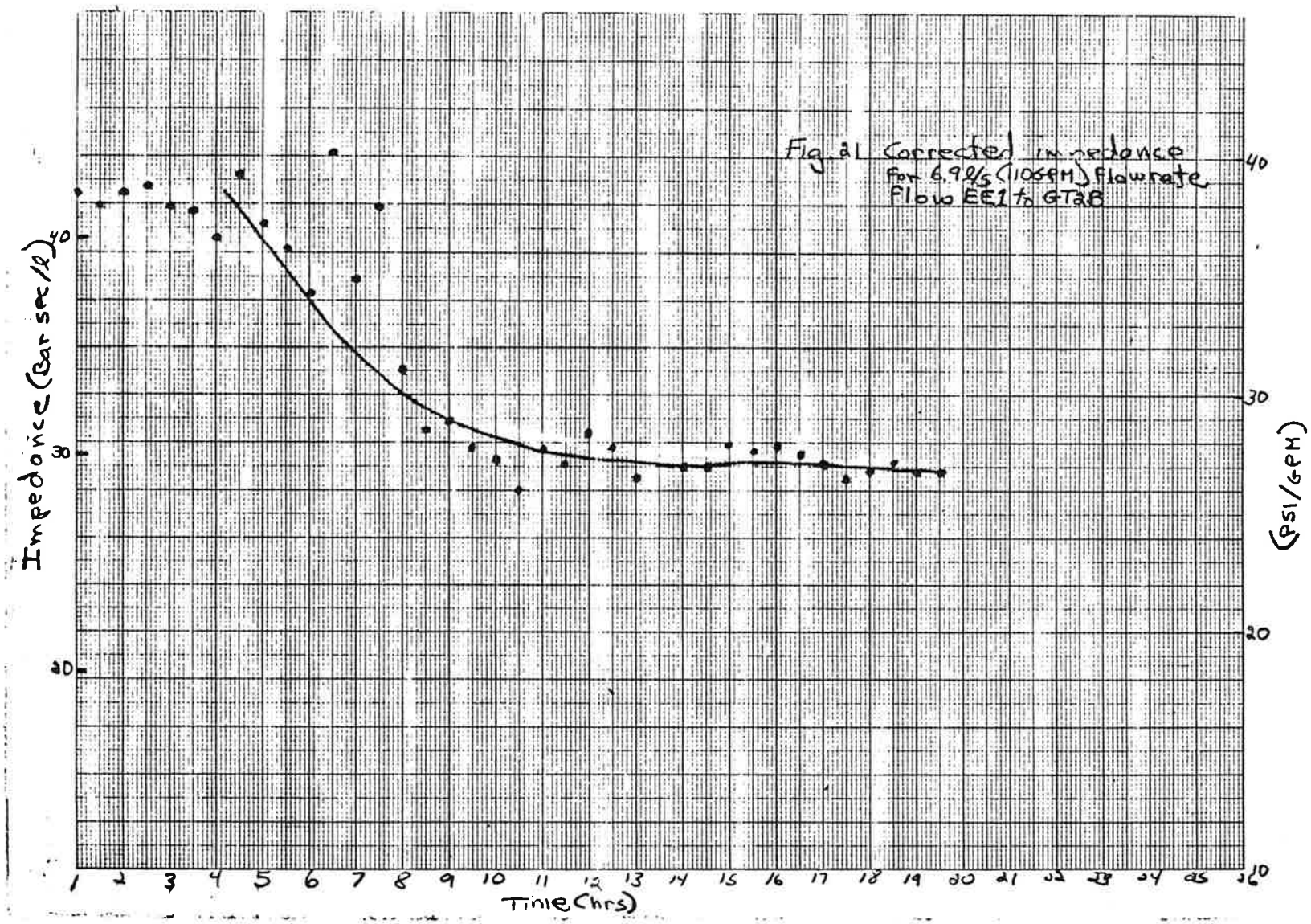

Fig. 21 Corrected impedance for 6.9 l/s (109 GPM) flowrate flow EE1 to GT2B

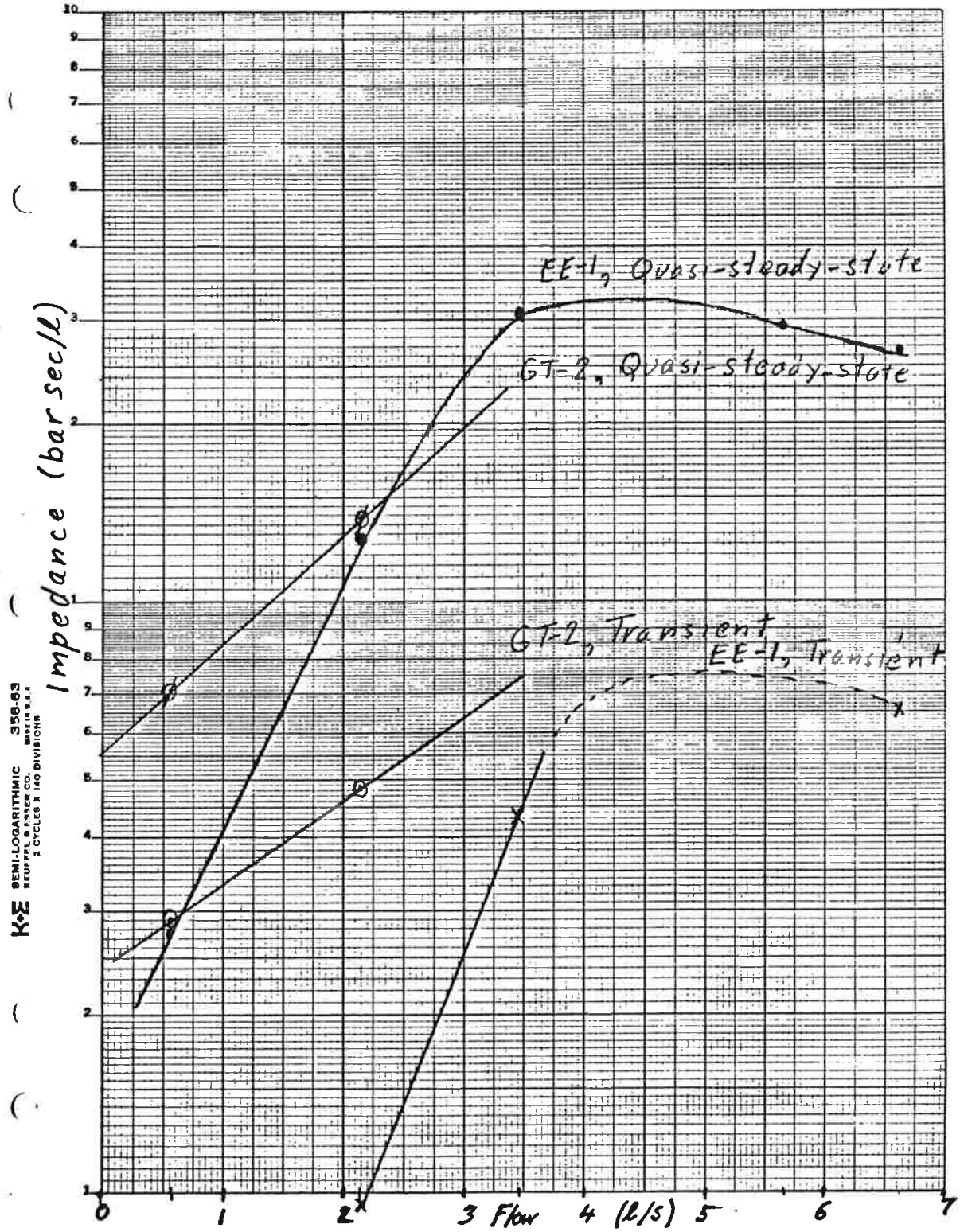

Fig. 22 Flow dependence of impedance.